A&A 563, A1 (2014)
DOI: 10.1051/0004-6361/201322738

Astronomy & Astrophysics

Orbit and properties of the massive X-ray binary BD +60 73=IGR J00370+6122⋆

J. H. Grunhut[1], C. T. Bolton[2], and M. V. McSwain[3]

[1] European Southern Observatories, Karl-Schwarzschild-Str. 2, 85748 Garching, Germany
e-mail: jgrunhut@eso.org
[2] Department of Astronomy and Astrophysics, University of Toronto, 50 St. George St., Toronto M5S 3H4, Canada
[3] Department of Physics, Lehigh University, 16 Memorial Drive East, Bethlehem PA 18015, USA
e-mail: mcswain@lehigh.edu

Received 24 September 2013 / Accepted 1 January 2014

ABSTRACT

Context. High-energy X-rays generated in massive binary systems can arise from several different mechanisms. Constraints on the orbital parameters of these systems are therefore necessary to properly understand and interpret the X-ray phenomena.
Aims. In this study we aim to determine a spectroscopic orbit for the high-mass X-ray binary system BD +60 73=IGR J00370+6122, to infer the properties of the optical and compact companion, and to interpret the characteristics of the X-ray light curve within the context of our findings.
Methods. We acquired 123 spectroscopic observations with the *David Dunlap* Observatory and Kitt Peak National Observatory telescopes in the optical domain. Using a cross-correlation technique, we measured the radial velocity of each of these spectra relative to the heliocentric rest-frame. An orbital solution was obtained from the resulting radial velocity measurements. Spectra of several spectral standards were also acquired to reassess the spectral classification of the optical companion.
Results. The best-fit orbital parameters suggest an eccentricity of $e = 0.48^{+0.02}_{-0.03}$ and a mass-function of $f(M) = 0.009 \pm 0.002$, lending further support to the assumption that the companion is a low-mass compact star. We find that the X-ray maximum occurs just after the time of periastron passage, but before the time of superior conjunction when the optical companion could eclipse the compact companion. The spectrum of the optical companion is best matched by the B1Ib spectral standard HD 24398, which reaffirms the original classification.
Conclusions. The mass-function combined with a plausible range of possible masses for a neutron star companion yields primary masses within the range expected for the spectral type of BD +60 73 for high orbital inclinations. The compact companion cannot be a black hole unless the supergiant has an exceptionally high mass for its B1Ib spectral type or if the inclination of its orbit is very low. The X-ray timing and characteristics can potentially be explained by accretion variations on the compact object; but this would require the companion to be a magnetar.

Key words. techniques: radial velocities – techniques: spectroscopic – ephemerides – stars: magnetars – binaries: general – stars: individual: BD+60 73

1. Introduction

Our attention was first drawn to the B1Ib star BD +60 73 as the optical counterpart of IGR J00370+6122 by den Hartog et al. (2004). Rutledge (2004) had previously associated BD +60 73 with 1RXS J003709.6+612131 = IGR J00370+6122 with a 99.7 per cent probability based on the spatial coincidence. BD +60 73 had previously been identified as the optical counterpart to 1RXS J003709.6+612131 (Rutledge 2000). den Hartog et al. (2004) reported periodically variable hard X-ray emissions that occurred with a period of 15.665 ± 0.006 d and suggested that this was the result of an eccentric binary where a compact object was passing through the denser part of the wind of the B star at periastron. A more detailed X-ray analysis was carried out by in't Zand et al. (2007), who further constrained the period to 15.6627 ± 0.0042 d while also identifying a possible 346 ± 6 s period that was proposed to be due to the spin of a pulsar companion.

The details of the X-ray results based on the analyses of den Hartog et al. (2006) and in't Zand et al. (2007) suggest that the epoch of maximum flux is MJD 53 001.7 ± 0.3 and that the X-ray emission varies by at least a factor of 6. The folded light curve shows a single-peak flux from RXTE-ASM of 3.3 mCrab, and remains higher than 2 mCrab for approximately 3 d before reaching a quiescent level lower than 1 mCrab. The average X-ray light curve has an asymmetric peak with a faster rise to maximum followed by a slower decline.

Originally classified as a B1Ib star by Morgan et al. (1955), Reig et al. (2005) reclassified the optical companion star BD +60 73 as B0.5II-III based on medium-resolution spectra and a comparison with the B0.5III spectral standard HD 218376 (1 Cas). Their main reasoning for this classification was the presence of He II λ4686, the only He II line identified. Reig et al. (2005) also noted the lack of emission in He I or Hα spectral lines, which indicates that this star has not entered a Be phase, and that N lines appeared to be enhanced although C was not depleted, suggesting the accretion of CNO during an earlier evolution stage from the compact companion.

Our goal was to obtain a spectroscopic orbit for the binary system, to reassess the spectral classification and distance determination, and to learn as much as we could about the physical properties of the system from these analyses.

⋆ Table 2 is available in electronic form at http://www.aanda.org

Table 1. Details of the different instrument configurations.

Instrument configuration	$\frac{\lambda}{\Delta\lambda}$	λ_c (Å)	$\Delta\lambda$ (Å/pix)	Spec. wind.
Thomson 1800G	11 000	6600	0.194	200 Å
Thomson 1800G	11 000	4686	0.206	200 Å
Thomson 600C	2500	4650	0.616	650 Å
Jobin-Yvon 600C	2500	4650	0.438	900 Å
KPNO Coudé feed	~12 000	6750	0.217	650 Å

Notes. Listed are the configuration of the instrument, the spectral dispersion ($\lambda/\Delta\lambda$), the central wavelength (λ_c), the one-pixel CCD resolution ($\Delta\lambda$), and the width of the spectral window for the given instrumental setup.

2. Observations and reductions

A total of 96 spectroscopic observations of BD +60 73 were obtained using the 1.88-m Cassegrain telescope at the *David Dunlap* Observatory (DDO) between 2004 and 2006. The spectra were recorded with a Thomson 1024 × 1024 pixel CCD with 19 μm pixels and a Jobin-Yvon 2048 × 512 pixel CCD with 13.5 μm pixels using either the high-resolution 1800 l/mm (1800G) or low-resolution 600 l/mm (600C) grating. The spectra were bias subtracted, flat fielded, and wavelength calibrated using standard routines in IRAF[1]. The spectra were wavelength calibrated using FeAr comparison lamp spectra taken immediately before and after each set of exposures. Continuum normalisation was accomplished within IRAF using the CONTINUUM task with a fourth-order or an eighth-order Legendre polynomial fit to line-free regions for the spectra obtained with the 1800G or the 600C grating, respectively.

An additional 27 useable spectra were obtained with the Kitt Peak National Observatory (KPNO) Coudé feed telescope over a period of 33 nights between 2008 October and November. The spectra were acquired and reduced in an identical manner to Aragona et al. (2009). Listed in Table 1 are the different instrumental configurations and the associated properties of each setup.

For each spectrum we measured the signal-to-noise ratio (S/N) by determining the root-mean-square (RMS) scatter about the continuum in a line-free region. The measured S/N for the high-resolution 1800G DDO blue spectra are quite low at ~25, while the low-resolution 600C DDO spectra have a much higher S/N of ~100. Note that the S/N varies by approximately 50 per cent towards the bluest regions compared to the reddest region where the S/N was measured for the 600C spectra. The S/N for the KPNO data and the DDO red data were measured in the region surrounding the He I λ6678 spectral line and have an average of ~60 and ~120, respectively.

The high-resolution 1800G spectra in the red contain only two prominent stellar absorption features, Hα and He I λ6678, although a weak N II λ6482 is also distinguishable above the noise in some of our spectra. Weak emission is visible in the red wing of Hα (reaching a peak of ~1.1 times the continuum flux) in all the DDO spectra (and KPNO), but no measurable variability is found in Hα; this is consistent with the previous findings of Reig et al. (2005) that this is not a Be star. The KPNO data cover a much broader spectral range, but like in the DDO red data, Hα and He I λ6678 are the most prominent absorption lines. The high-resolution DDO blue spectra also only cover a narrow spectral range with few absorption lines present – for instance, Si III λ4567, the O II λ4649 triplet, and He I λ4713. The low-resolution 600C DDO spectra cover a substantially broader spectral range, with many prominent absorption lines usable for radial velocity measurements. Example spectra obtained with each configuration are shown in Fig. 1.

[1] IRAF is distributed by the National Optical Astronomy Observatory, which is operated by the Association of Universities for Research in Astronomy, Inc., under cooperative agreement with the National Sciences Foundation.

3. Radial velocities and orbital elements

The wavelength scale of all spectra was shifted to the barycentre of the solar system prior to any radial velocity measurements. Radial velocities were measured by cross-correlating the observed spectra with a best-fit TLUSTY model ($T_{\rm eff}$ = 24 000 K and $\log(g)$ = 3.0; Hubeny & Lanz 1995), using the IRAF task FXCOR. The models were taken from the 2006 B-star grid for supergiants (Lanz & Hubeny 2007); but we note that the choice of model made little difference for our measured velocities. The hydrogen Balmer lines and diffuse interstellar band regions were ignored during the cross-correlation for the blue spectra to avoid any possible systematic offsets due to emission or outflows. Only the He I λ6678 line was used to measure radial velocities for the red spectra sampled from the DDO and KPNO datasets. In each case a Gaussian fit was used within FXCOR to determine the central peak and associated radial velocity uncertainties. Since BD +60 73 is expected to only have a moderate wind (and there is no evidence to the contrary), we do not expect to find large systematic differences between spectral lines formed at different optical depths. This was easily verified because we obtained similar radial velocity measurements from the cross-correlation of the different spectra using one observation as the template spectrum. Table 2 lists the measured radial velocities and associated properties for each observation.

Since the X-ray data were obtained with much higher cadence than our spectroscopic observations, we adopted the X-ray period of 15.6627 ± 0.0042 d (in't Zand et al. 2007) for our analysis after verifying that our measured velocities coherently varied with this period.

The orbital elements were calculated using a least-squares minimisation code. This code allows for systematic offsets between different datasets, which for our analysis corresponded to the different instrumental configurations. All 600C grating spectra were combined into a single dataset, while the other instrumental configurations composed of the DDO 1800 G He I measurements, the 1800 G λ_c = 4686 Å DDO data, and the KPNO data provided the remaining datasets for this analysis. The final best-fit parameters from our fitting routine are listed in Table 3 and were computed for the allowed orbital period 15.6627 ± 0.0042 d. The resulting orbital parameters are listed in Table 3 and the observed minus corrected values (O−C) are listed in Table 2. A standard error of 4.49 km s^{-1} is achieved from this fit. We note that the uncertainties listed in Table 3 may be larger than expected because of the relatively imprecise orbital period. In our final fits, we found a slight difference (~2 km s^{-1}) between the DDO datasets, but a much larger systematic offset (>10 km s^{-1}) between the DDO data and the KPNO data. We adopted a centre-of-mass velocity (γ) of −81 km s^{-1} from the DDO 600C dataset for the rest of our analysis since this represented our largest dataset and was consistent with all the DDO data. After correcting each dataset to the adopted centre-of-mass velocity we obtained the radial velocity curve shown in Fig. 2. An illustrative diagram showing the orbital geometry is

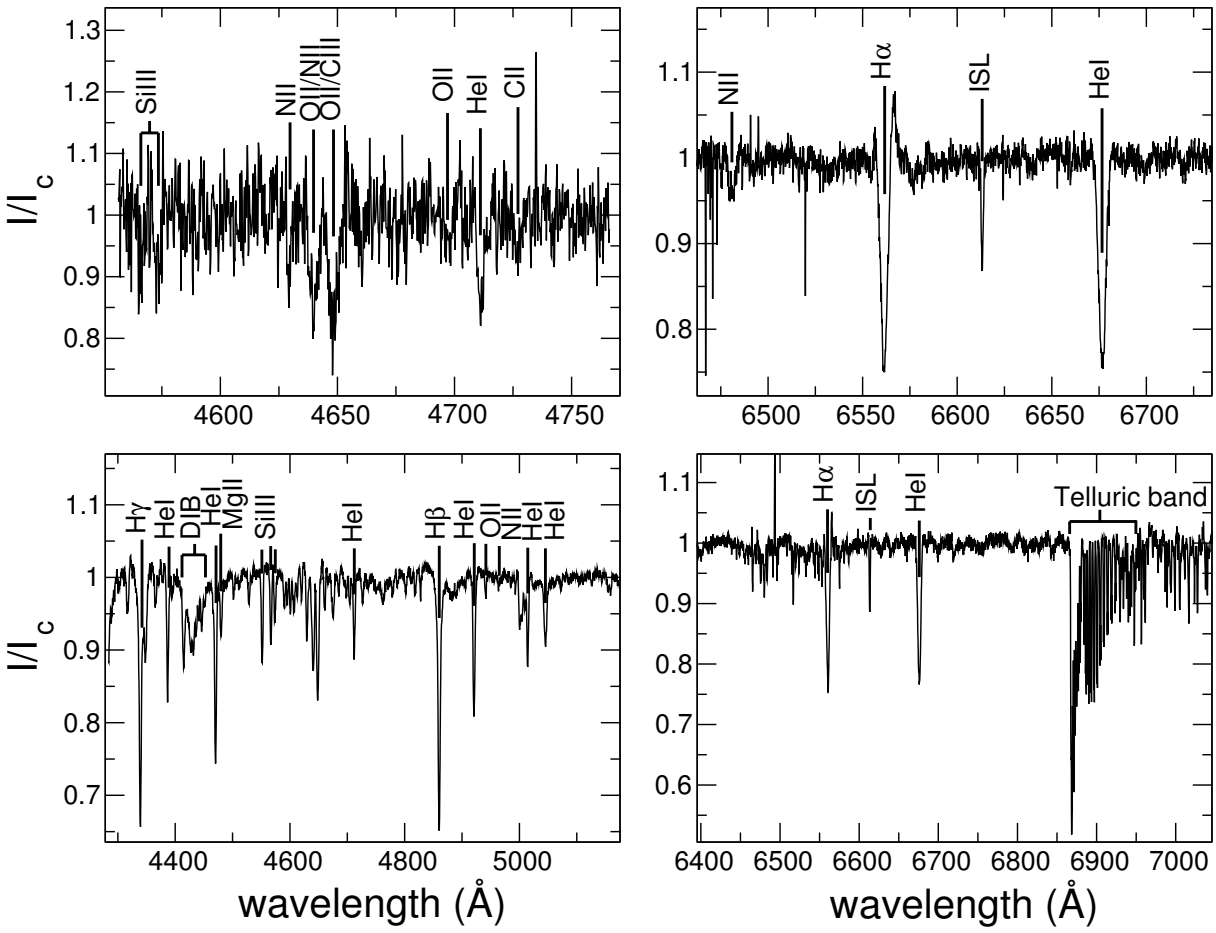

Fig. 1. Example spectra of BD +60 73 taken with different instrument configurations. Major spectral features are indicated as well as prominent interstellar lines (ISL) and diffuse interstellar bands (DIB). The narrow emission features are residual cosmic rays that were failed to be removed during reduction. *Top left*: DDO 1800 G, *top right*: DDO 1800 G, *bottom left*: DDO 600C, *bottom right*: KPNO Coudé.

Table 3. Orbital parameters of BD +60 73.

Parameter	Best fit
P (d)	15.6627 ± 0.0042^{a}
T_0 (HJD-2 450 000)	3000.04 ± 0.34
e	$0.48^{+0.02}_{-0.03}$
ω (deg)	167 ± 6
K_1 (km s^{-1})	19 ± 2
γ_1 (km s^{-1})	-79 ± 12
γ_2 (km s^{-1})	-81 ± 3
γ_3 (km s^{-1})	-77 ± 2
γ_4 (km s^{-1})	-68.7 ± 0.5
$f(m)$ ($M_\odot$)	0.009 ± 0.002
$a_1 \sin i$ (km)	$3.8 \pm 0.3 \times 10^6$
σ (km s^{-1})	4.49

Notes. Included are the period (P), the time of periastron (T_0), the eccentricity (e), the angle of the line of nodes (ω), the velocity semi-amplitude (K_1), the centre-of-mass velocity for the different instrument configurations (γ_1 = DDO 1800G, γ_2 = DDO 600C, γ_3 = DDO He I, γ_4 = KPNO He I), the mass-function ($f(M)$), the projected semi-major axis ($a_1 \sin i$), and the standard error of the fit (σ). γ_2 is adopted as the centre-of-mass velocity, as discussed in the text. [a] Fixed.

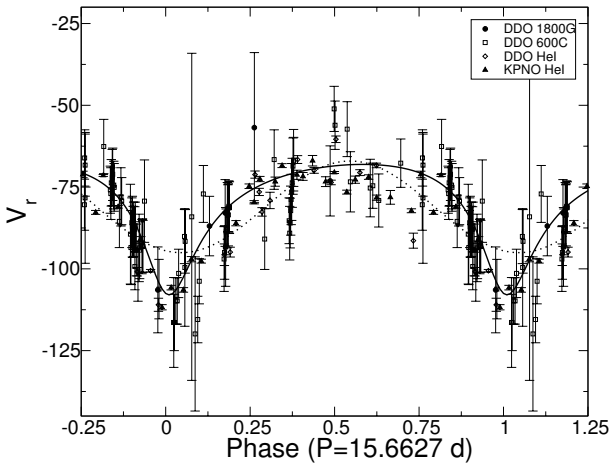

Fig. 2. Radial velocity curve of BD +60 73. Observations corresponding to the various instrument configurations are indicated by the symbols listed in the key and shown with their 1σ uncertainties. The best-fit theoretical curve is shown as the solid line, while the best-fit circular orbit is shown as the dashed line. Phase 0.0 corresponds to periastron.

provided in Fig. 3, which also indicates the phases of periastron, apastron, and inferior and superior conjunction.

Because it is of particular interest, we highlight the fact that our orbital solution confirms the expectations of den Hartog et al. (2004) that this is an eccentric binary system ($e = 0.48^{+0.002}_{-0.003}$). To additionally establish the robustness of this result we also computed a best-fit model assuming no eccentricity (which is also presented in Fig. 2). A circular orbit provides a much poorer fit to the observed radial velocity measurements (as evident from our uncertainty estimates of the eccentricity). The

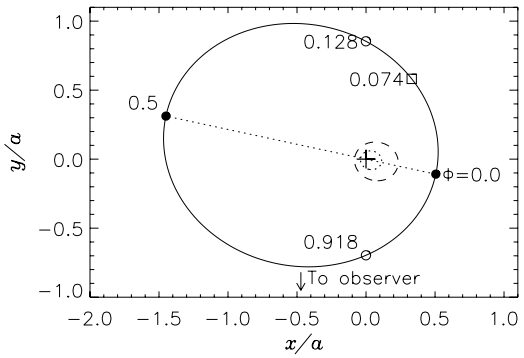

Fig. 3. Orbital geometry of BD +60 73, as seen when looking down on the orbital plane, with the compact companion's orbit indicated by the solid line in relative units. The dotted and dashed lines correspond to the orbits that the optical companion would have if the compact companion had a mass of 1.7 $M_\odot$ ($i = 90°$; dotted) or 3.5 $M_\odot$ ($i = 30°$; dashed), both corresponding to a mass $M \sim 22\,M_\odot$ for the optical companion, as suggested in Sect. 5. The centre-of-mass of the system is marked by the cross, and the position and phases of periastron and apastron (solid circles) and superior and inferior conjunction (open circles) along with the phase corresponding to maximum X-ray flux (open square) are also labelled.

goodness-of-fit (χ^2/ν) obtained from our best-fit model is considerably better ($\chi^2/\nu = 15.1$) than the best fit achieved with a solution assuming a circular orbit ($\chi^2/\nu = 60.1$). The high goodness-of-fit ($\chi^2/\nu \gg 1$) can mostly be attributed to the relatively low, and very likely underestimated, uncertainties obtained from the two red He I region datasets, since the cross-correlation was effectively obtained from a single line. The goodness-of-fit obtained without these measurements is more reasonable with values of 0.99 for the eccentric-orbit model and 5.2 for the circular-orbit model.

4. Spectral classification and related matters

BD +60 73 was originally classified as B1Ib by Morgan et al. (1955) by comparison with a carefully selected set of standard stars. More recently, Reig et al. (2005) reclassified this star by extrapolation from a single standard BN0.5II-III star. Classification from a single spectral standard may lead to erroneous results.

We therefore set out to re-classify the spectrum of BD +60 73 by comparing its spectrum with the spectra of a coarse grid consisting of the Morgan & Keenan (1973) anchor point standards in the wavelength range 3800 Å–5100 Å that were also observed with the DDO telescope. To compare the different spectra we divided the spectrum of BD +60 73 by each of the anchor point spectra, after shifting the latter to the same velocity as BD +60 73 and removing the diffuse interstellar bands from all spectra. To quantify the agreement between the different spectra we computed the RMS difference for each divided spectrum to determine the best fit. A comparison between BD +60 73 and the spectral standards is shown in Fig. 4. The ratio with HD 24398, the B1Ib standard, had the lowest RMS. Lower-luminosity standard stars all had hydrogen lines that were too strong to match BD +60 73. A line-by-line comparison of the B1Ib standard with BD +60 73 showed that the He II λ4686 line is slightly stronger and the O II lines are slightly weaker in the spectrum of BD +60 73. This suggests that its spectral type may be slightly earlier than B1, which is also somewhat supported by our TLUSTY model fits to the spectra (measured $T_{\rm eff} = 24$ kK, but expected $T_{\rm eff} = 22$ kK; Searle et al. 2008). However, we adopt B1Ib until we can obtain a finer grid of standard stars for comparison.

We hold the suggestion of Reig et al. (2005) that BD +60 73 belongs to the "far" group of Cas OB5 to be unlikely because of the large angular separation between the star and the association. It is much more likely to be associated with Cas OB4, as suggested by Humphreys (1978). However, we caution that an argument can be made that BD +60 73 can be a member of either Cas OB7 or Cas OB1, which are slightly closer to us than Cas OB4.

Humphreys (1978) reported a distance modulus of 12.3 for Cas OB5, which yields $M_V = -5.0$ for BD +60 73. This agrees well with the absolute magnitude derived from HIPPARCOS data for type Ib supergiants, $M_V = -4.47$ for B1-B1.5 stars, and $M_V = -5.29$ for B0-B0.5 stars (Wegner 2006). The distance modulus of Humphreys (1978) corresponds to $d = 2.9$ kpc, which is consistent with the interstellar reddening of BD +60 73, so there is little doubt that it is a luminous massive star.

5. Discussion

Based on our orbital solution, we find that the X-ray peak occurs approximately ~1.1 days after periastron. The general shape of the X-ray light curve cannot be explained by the B star eclipsing the compact object, even if the orbital inclination is 90°, because the time of superior conjunction is expected to occur at phase 0.128 = 2.0 days after periastron. On the other hand, the shape of the X-ray light curve can be explained by the neutron star's brief transition from an ejector mode to an accretor or propeller mode near periastron. We can estimate the physical length scales of the neutron star using our measured orbital parameters and spectral type for BD +60 73, typical stellar and wind parameters for B1Ib supergiants (Searle et al. 2008), and a β-law velocity profile for the stellar wind (Howarth & Prinja 1989; Puls et al. 1996).

We find that the relative velocity between the neutron star's eccentric orbit and the stellar wind, $V_{\rm rel}$, reaches a minimum shortly after periastron at $\phi = 0.05$. Despite the faster orbital velocity near periastron, the wind is less accelerated close to the star. Assuming a typical mass of the neutron star $M_2 = 1.4\,M_\odot$, the accretion radius of the neutron star

$$R_{\rm a} = \frac{2GM_2}{V_{\rm rel}^2} \tag{1}$$

thus varies between 5.3×10^{10} cm $\lesssim R_{\rm a} \lesssim 2.3 \times 10^{11}$ cm, with the maximum at $\phi = 0.05$. The corotation radius of the neutron star is

$$R_{\rm c} = \left(\frac{GM_2}{\omega^2}\right)^{1/3} = 2.8 \times 10^{10}\,{\rm cm}. \tag{2}$$

Here, the rotational frequency of the neutron star, ω, is determined from the proposed pulsation period of 346 ± 6 s (in't Zand et al. 2007). The magnetospheric radius, or Alfvén radius, can be determined by equating the ram pressure of the inflowing gas to the magnetic field pressure:

$$R_{\rm mag} = \left(\frac{\mu^2}{2S_{\rm a}\sqrt{2GM_2}}\right)^{2/7}, \tag{3}$$

where μ is the magnetic moment and $S_{\rm a}$ is the accretion rate. $S_{\rm a}$ should peak shortly after periastron due to the slower $V_{\rm rel}$ and higher wind density near the star. Thus, $R_{\rm mag}$ is most likely variable during the orbit, with a decrease near periastron.

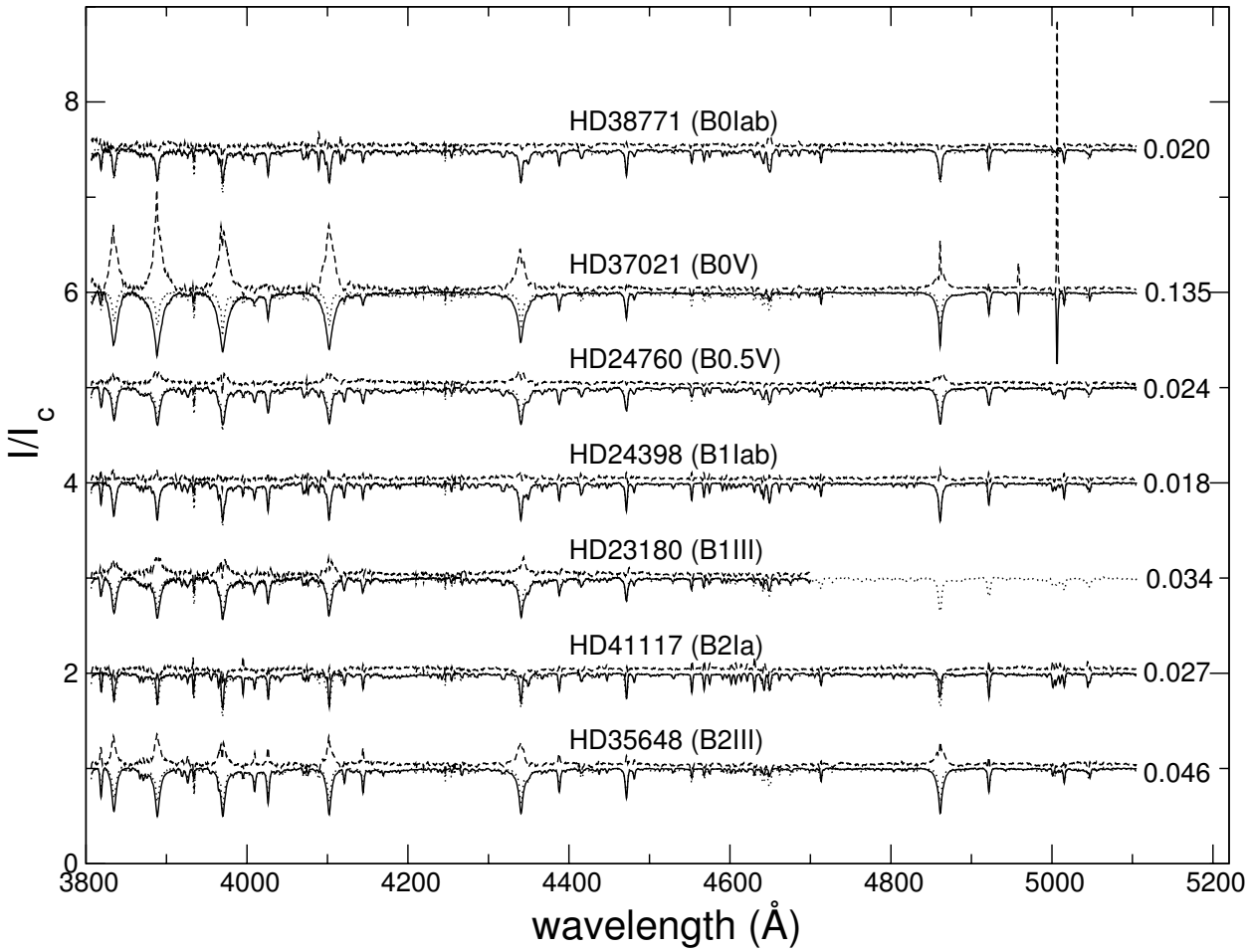

Fig. 4. Comparison of the spectra of BD +60 73 (dotted line) with several spectral standards (solid line). The ratio of BD +60 73 with each of the spectral standards is also shown (dashed line). The spectra are offset for clarity, with the measured RMS of the ratioed spectra indicated on the right.

The neutron star will be an accretor if $R_{\rm mag} < R_{\rm a}$ and $R_{\rm mag} < R_{\rm c}$. It will be in propeller mode if $R_{\rm c} < R_{\rm mag} \leq R_{\rm a}$, and it will be an ejector if $R_{\rm mag} > R_{\rm c}$ and $R_{\rm mag} > R_{\rm a}$. Since X-rays are not observed during most of the orbit, we rule out $R_{\rm mag} < R_{\rm c}$ generally. However, if $R_{\rm mag} \sim 10^{10}$ to 10^{11} cm, the neutron star may transition from an ejector mode to accretion or propeller mode as $R_{\rm a}$ increases and $R_{\rm mag}$ decreases during a brief window just after periastron. Such a high value of $R_{\rm mag}$ is only possible if the neutron star has a very high $\mu \sim 10^{33}\,{\rm G\,cm^3}$ (corresponding to a magnetar with magnetic field strength $B \sim 10^{15}$ G) and/or very inefficient accretion. The neutron star is likely not observable as a radio pulsar during the ejector mode due to high extinction by the stellar wind of the supergiant (e.g. McSwain et al. 2011).

The mass of BD +60 73 is probably $\sim 22\,M_\odot$ based on its spectral classification and inferred luminosity (Searle et al. 2008). The proposed pulsar spin period (in't Zand et al. 2007) and the unusual X-ray light curve suggest that the compact companion is a neutron star. X-ray emission from black holes is known to switch from high/low and soft/hard emission states, but the X-ray emission is not known to correlate with orbital phase (Homan & Belloni 2005). Taking this into account Fig. 5 presents the possible range of masses for each component of the binary system for different orbital inclinations. The horizontal dashed lines in Fig. 5 show a reasonable range for the upper and lower limits for neutron star masses according to Lattimer & Prakash (2005, and references therein). The slanted lines in Fig. 5 show the 1σ and 3σ upper and lower bounds for the position of the $i = 60°$ line in the M_1–M_2 plane. Clearly, a high orbital inclination is favoured if the compact object is a neutron

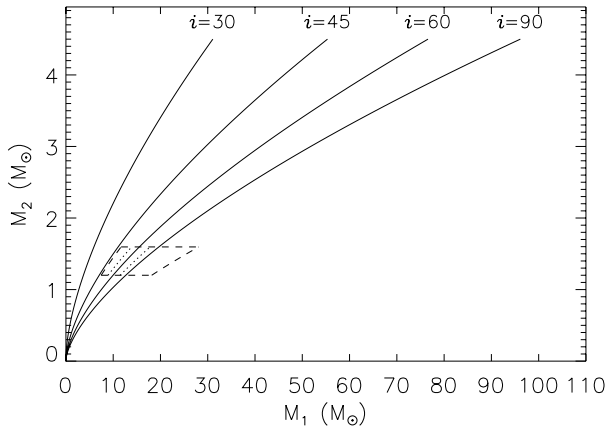

Fig. 5. $M_1 - M_2$ phase space diagram showing the possible mass ranges for BD +60 73 (M_1) and the compact secondary (M_2) for a variety of orbital inclinations using the derived mass function of $f(M/M_\odot) = 0.009 \pm 0.002$. The slanted dotted and dashed lines outline the 1σ and 3σ upper and lower bounds for the possible mass of the primary for $i = 60°$. The horizontal dashed lines show a reasonable range for the upper and lower mass-limits of a neutron star (Lattimer & Prakash 2005).

star with a typical mass. If such a high inclination were true, one would expect to see evidence of this in the X-ray light curve at the predicted phase of superior conjunction (phase 0.128). There is a considerable drop in the X-ray flux around this phase (in't Zand et al. 2007), but it is challenging to attribute this to an eclipse event based on our previous discussion. On the other hand, if no eclipsing occurs in the X-ray light curve we can establish an upper limit on the orbital inclination of $i \lesssim 72°$ using the 3σ limits of our orbital parameters and the typical stellar radius of a B1Ib supergiant ($\sim 35\,R_\odot$; Searle et al. 2008). We cannot rule out the possibility that the secondary is a black hole, but even a minimal-mass black hole requires a low inclination orbit. If the compact companion is not a black hole, we can establish a lower limit on the allowed orbital inclination of $i > 48°$ using the 3σ limits of our mass function if we assume an upper limit on the neutron star mass of $1.6\,M_\odot$, or $i > 41°$ if $M_2 < 1.8\,M_\odot$.

As already pointed out by in't Zand et al. (2007), the orbital period (15.6627 d) and pulsar period (346 s) are remarkably similar to the X-ray transient system SAX J2103.5+4545 (Hulleman et al. 1998; Baykal et al. 2000). The RXTE X-ray data of both systems show a similar single-peaked light curve with a sharp rise-time followed by a slow decay (Baykal et al. 2000). From the optical data we also find that the derived eccentricity (~0.48) for BD +60 73 agrees well with the eccentricity estimated for that system (0.4 ± 0.2).

According to Sitnik (2003), the radial velocity of Cas OB4 with respect to the local standard of rest (LSR) is $-29.1\,\mathrm{km\,s^{-1}}$. If BD +60 73 is associated with Cas OB4, it has a radial velocity of $62\,\mathrm{km\,s^{-1}}$ with respect to the association. The proper motion of BD +60 73 is not statistically significant (Tycho 2 catalogue; Høg et al. 2000). If the supernova explosion that produced the compact object in this high-mass X-ray binary was symmetric, we would expect that the centre-of-mass velocity of the resulting system would be accelerated along the major axis of the resulting orbit without altering the inclination of the orbit. Thus the large space motion of BD +60 73 along the line of sight is consistent with a high inclination orbit, and we conclude that the compact secondary is almost certainly a neutron star.

6. Conclusions

From the radial velocities measured from spectra obtained with the DDO and KPNO telescopes, we confirmed that BD +60 73 is a single-line spectroscopic binary with the same orbital period as the X-ray period of ~15.66 d. From our fits to the radial velocities, we found that this system has an eccentricity of $e = 0.48^{+0.02}_{-0.03}$ and that the time of periastron occurs roughly 1.1 d before the X-ray maxima. We confirmed the spectral classification of B1Ib as previously found by Morgan et al. (1955), which results in a primary mass of $\sim 22\,M_\odot$ using the results of Searle et al. (2008). Our derived mass function combined with a plausible range of possible masses for the secondary strongly suggests that the companion is a neutron star (confirming the results of in't Zand et al. 2007). Since no clear evidence exists for an eclipse event, we established that we are viewing this system at an orbital inclination of $i \lesssim 72°$. Lastly, we proposed that if the compact companion is a magnetar, it could account for the characteristics of the X-ray light curve and the timing of the X-ray maximum relative to the time of periastron; follow-up observations to infer its magnetic field strength should resolve this mystery.

Acknowledgements. The authors thank the anonymous referee for useful improvements. J.H.G. was formerly supported by an Ontario Graduate Scholarship and an Alexander Graham Bell Canada Graduate Scholarship from the Natural Sciences and Engineering Research Council of Canada (NSERC). C.T.B.'s research was partially supported by a Discovery Grant from NSERC. M.V.M. is supported by the National Science Foundation under grant AST-1109247 and an institutional grant from Lehigh University.

References

Aragona, C., McSwain, M. V., Grundstrom, E. D., et al. 2009, ApJ, 698, 514
Baykal, A., Stark, M. J., & Swank, J. 2000, ApJ, 544, 129
den Hartog, P. R., Kuiper, L. M., Corbet, R. H. D., et al. 2004, ATel, 281, 1
den Hartog, P. R., Hermsen, W., Kuiper, L., et al. 2006, A&A, 451, 587
Homan, J., & Belloni, T. 2005, Ap&SS, 300, 107
Howarth, I. D., & Prinja, R. K. 1989, ApJS, 69, 527
Høg, E., Fabricius, C., Makarov, V. V., et al. 2000, A&A, 355, L27
Hubeny, I., & Lanz, T. 1995, ApJ, 439, 875
Hulleman, F., in't Zand, J. J. M., & Heise, J. 1998, A&A, 337, 25
Humphreys, R. M. 1978, ApJS, 38, 309
in't Zand, J. J. M., Kuiper, L., den Hartog, P. R., Hermsen, W., & Corbert, R. H. D. 2007, A&A, 469, 1063
Lanz, T., & Hubeny, I. 2007, ApJS, 169, 83
Lattimer, J. M., & Prakash, M. 2005, Phys. Rev. Lett., 94, 1101
McSwain, M. V., Ray, P. S., Ransom, S. M., et al. 2011, ApJ, 738, 105
Morgan, W. W., & Keenan, P. C. 1973, ARA&A, 11, 29
Morgan, W. W., Code, A. D., & Whitford, A. E. 1955, ApJS, 2, 41
Puls, J., Kudritzki, R.-P., Herrero, A., et al. 1996, A&A, 305, 171
Reig, P., Negueruela, I., Papamastorakis, G., Manousakis, A., & Kougentakis, T. 2005, A&A, 440, 637
Rutledge, R. E. 2004, ATel, 282, 1
Rutledge, R. E., Brunner, R. J., Prince, T. A., & Lonsdale, C. 2000, ApJS, 131, 335
Searle, S. C., Prinja, R. K., Massa, D., & Ryans, R. 2008, A&A, 481, 777
Sitnik, T. G. 2003, Astron. Lett., 29, 311
Wegner, W. 2006, MNRAS, 371, 185

Pages 7 to 8 are available in the electronic edition of the journal at http://www.aanda.org

Table 2. Radial velocity measurements.

HJD (2 450 000+)	Grating	λ_c (Å)	S/N	V_r (km s^{-1})	σ_r (km s^{-1})	$O-C$ (km s^{-1})
3233.6243	1800G	4686	28	–91.7	7.9	–4.8
3234.6213	1800G	4686	24	–103.9	13.1	–0.4
3237.7419	1800G	4686	24	–80.4	10.2	1.6
3242.6114	1800G	4686	21	–70.6	10.7	–1.9
3252.6784	1800G	4686	24	–84.4	9.1	3.3
3254.7602	1800G	4686	13	–54.3	22.8	21.1
3280.5452	600C	4650	120	–99.3	7.1	–10.8
3286.5631	600C	4650	103	–90.9	9.3	–14.6
3307.5134	600C	4650	57	–79.1	8.1	–8.3
3321.7140	600C	4650	103	–57.3	8.4	13.4
3322.7824	600C	4650	177	–75.3	8.8	–4.7
3402.5095	600C	4650	199	–67.7	7.4	3.9
3486.7955	600C	4650	7	–84.1	52.0	15.7
3509.8125	600C	4650	121	–73.4	9.2	–2.7
3510.8523	600C	4650	144	–74.6	6.9	–3.9
3522.8457	600C	4650	135	–67.3	7.5	6.0
3528.8188	600C	4650	82	–66.1	8.6	7.4
3528.8410	600C	4650	79	–68.3	9.5	5.3
3545.6726	600C	4650	95	–75.8	7.2	2.5
3545.6950	600C	4650	82	–77.0	7.9	1.4
3545.7173	600C	4650	97	–73.7	7.1	4.8
3545.7608	600C	4650	118	–72.1	8.6	6.7
3545.7834	600C	4650	117	–71.1	8.0	7.8
3545.8311	600C	4650	125	–74.4	7.3	4.8
3545.8497	600C	4650	106	–75.1	7.3	4.3
3546.6041	600C	4650	63	–89.4	15.2	–3.4
3546.6267	600C	4650	66	–93.5	11.3	–7.2
3546.6717	600C	4650	72	–85.9	7.6	0.9
3546.6941	600C	4650	86	–87.1	9.3	0.0
3546.7320	600C	4650	88	–88.7	7.8	–1.2
3546.7542	600C	4650	95	–87.9	8.3	–0.1
3546.8052	600C	4650	86	–87.9	6.9	0.6
3546.8276	600C	4650	195	–86.8	7.2	2.0
3548.6130	600C	4650	57	–116.4	13.8	–6.6
3548.6357	600C	4650	80	–116.4	8.6	–6.8
3548.7060	600C	4650	155	–109.8	7.1	–0.7
3548.7757	600C	4650	130	–109.8	7.1	–1.4
3548.8397	600C	4650	146	–101.4	7.4	6.3
3549.6032	600C	4650	13	–119.9	23.7	–22.2
3549.7239	600C	4650	99	–115.5	7.1	–19.3
3549.7960	600C	4650	128	–103.8	6.9	–8.5
3561.7541	600C	4650	152	–85.5	8.0	–4.4
3561.8255	600C	4650	134	–78.0	8.9	3.7
3561.8615	600C	4650	124	–79.3	7.2	2.7
3562.6165	600C	4650	103	–100.7	9.2	–10.2
3562.6721	600C	4650	108	–93.6	10.3	–2.3
3562.6951	600C	4650	104	–94.3	8.7	–2.6
3562.8029	600C	4650	118	–93.2	8.3	0.2
3562.8252	600C	4650	151	–92.9	8.2	0.8
3562.8480	600C	4650	138	–93.1	7.9	1.0
3566.6085	600C	4650	56	–97.0	9.9	–12.2
3566.6308	600C	4650	71	–95.0	8.2	–10.3
3566.6815	600C	4650	89	–93.3	12.0	–9.0
3566.7052	600C	4650	91	–88.7	7.0	–4.5
3566.7624	600C	4650	97	–83.6	10.0	0.2
3566.7846	600C	4650	108	–81.5	7.2	2.2
3566.8070	600C	4650	103	–83.5	9.5	0.1
3566.8293	600C	4650	116	–80.9	7.8	2.5
3566.8572	600C	4650	112	–81.3	7.9	2.0
3569.6274	600C	4650	77	–85.3	7.0	–11.7
3569.6510	600C	4650	83	–89.1	8.2	–15.5

Notes. Listed are the heliocentric Julian date, the spectrograph used, the central wavelength of the observation, the inferred S/N in the continuum, the measured radial velocity, the uncertainty on the radial velocity measurement, and the difference between the observed and corrected radial velocity (O−C).

Table 2. continued.

HJD (2 450 000+)	Grating	λ_c (Å)	S/N	V_r (km s^{-1})	σ_r (km s^{-1})	$O-C$ (km s^{-1})
3569.6744	600C	4650	103	–86.0	7.6	–12.4
3569.6972	600C	4650	91	–82.2	7.5	–8.7
3569.7204	600C	4650	136	–78.8	7.7	–5.3
3569.7432	600C	4650	104	–76.5	8.7	–3.1
3569.7671	600C	4650	81	–73.7	7.5	–0.3
3569.8041	600C	4650	91	–68.6	8.6	4.7
3569.8297	600C	4650	96	–66.8	9.4	6.5
3575.7971	600C	4650	128	–80.4	7.8	–6.9
3575.8289	600C	4650	132	–78.3	20.2	–4.8
3609.9063	600C	4650	98	–79.3	12.6	16.0
3611.7622	600C	4650	66	–90.1	8.3	14.2
3611.7779	600C	4650	18	–99.6	18.0	4.5
3611.7926	600C	4650	70	–91.6	9.7	12.3
3612.6366	600C	4650	132	–77.1	8.7	16.0
3618.7005	600C	4650	162	–51.1	6.9	20.0
3618.7423	600C	4650	119	–56.1	7.4	14.9
3623.6806	600C	4650	166	–62.6	8.3	14.1
3751.5448	600C	4650	123	–106.2	9.1	0.7
3897.8479	600C	4650	125	–66.6	9.1	8.6
3162.7838	1800G	6600	31	–62.9	1.2	6.4
3176.8010	1800G	6600	49	–78.9	1.3	–5.9
3183.8180	1800G	6600	25	–87.7	2.3	–18.9
3192.8349	1800G	6600	22	–75.4	2.5	–3.4
3197.7665	1800G	6600	26	–64.7	0.7	2.3
3206.6511	1800G	6600	34	–91.2	1.5	–11.8
3212.6648	1800G	6600	85	–66.9	0.9	0.0
3218.6222	1800G	6600	68	–96.9	0.4	–0.3
3223.6598	1800G	6600	78	–72.8	1.1	0.6
3233.6651	1800G	6600	83	–97.2	1.3	–10.9
3234.6485	1800G	6600	81	–107.3	2.0	–4.5
3237.7076	1800G	6600	51	–92.0	3.3	–11.0
3242.6526	1800G	6600	80	–69.9	0.7	–2.4
3254.7889	1800G	6600	50	–67.5	1.1	6.6
3398.4950	1800G	6600	89	–66.2	0.9	2.0
3618.7833	1800G	6600	81	–56.7	1.0	10.6
4758.6332	KPNO Coudé	6750	124	–60.1	0.8	4.5
4759.6639	KPNO Coudé	6750	148	–56.0	0.6	5.9
4760.6305	KPNO Coudé	6750	126	–59.3	1.2	0.9
4761.6810	KPNO Coudé	6750	111	–60.9	1.5	–2.0
4762.6658	KPNO Coudé	6750	121	–64.1	0.6	–5.8
4763.6745	KPNO Coudé	6750	122	–59.5	0.7	–1.3
4764.6849	KPNO Coudé	6750	109	–65.7	2.1	–7.0
4765.6587	KPNO Coudé	6750	114	–69.8	0.6	–9.9
4766.6844	KPNO Coudé	6750	131	–70.3	0.6	–7.7
4767.7240	KPNO Coudé	6750	138	–68.6	0.4	–0.4
4768.7748	KPNO Coudé	6750	133	–78.5	0.8	1.5
4769.7591	KPNO Coudé	6750	109	–99.3	0.8	–3.1
4770.7524	KPNO Coudé	6750	96	–94.0	0.7	–1.4
4771.5784	KPNO Coudé	6750	120	–85.2	0.6	–3.4
4773.7999	KPNO Coudé	6750	104	–62.3	0.7	4.1
4776.7387	KPNO Coudé	6750	105	–54.5	1.6	5.1
4777.7497	KPNO Coudé	6750	108	–58.1	0.3	0.5
4778.7209	KPNO Coudé	6750	121	–60.3	1.1	–2.1
4779.7086	KPNO Coudé	6750	126	–65.8	0.8	–7.5
4781.7583	KPNO Coudé	6750	105	–58.7	1.0	2.2
4782.6986	KPNO Coudé	6750	102	–59.0	0.3	5.1
4785.8466	KPNO Coudé	6750	114	–93.3	0.7	4.6
4786.7858	KPNO Coudé	6750	130	–84.6	0.8	2.9
4788.8532	KPNO Coudé	6750	107	–73.6	0.8	–4.5
4789.6922	KPNO Coudé	6750	106	–67.2	0.5	–1.7
4790.6706	KPNO Coudé	6750	111	–60.9	1.4	1.7
4791.6768	KPNO Coudé	6750	117	–58.8	1.4	1.8